Centre for
Automotive Safety Research

The effect of bull bars on head impact kinematics in pedestrian crashes

RWG Anderson, S Doecke, AL van den Berg,
DJ Searson, G Ponte

CASR REPORT SERIES

CASR059

April 2009

THE UNIVERSITY
OF ADELAIDE
AUSTRALIA

Report documentation

REPORT NO.	DATE	PAGES	ISBN	ISSN
CASR059	April 2009	22	978 1 920947 60 6	1449-2237

TITLE

The effect of bull bars on head impact kinematics in pedestrian crashes

AUTHORS

RWG Anderson, S Doecke, AL van den Berg, DJ Searson, G Ponte

PERFORMING ORGANISATION

Centre for Automotive Safety Research
The University of Adelaide
South Australia 5005
AUSTRALIA

SPONSORED BY

Motor Accident Commission
GPO Box 1045
Adelaide SA 5001
AUSTRALIA

AVAILABLE FROM

Centre for Automotive Safety Research
http://casr.adelaide.edu.au/publications/researchreports

ABSTRACT

This study sought to assess the effect of bull bars on the head kinematics and head impact severity of an adult pedestrian in a collision. Multibody models were created to represent a range of sport-utility vehicles and common bull bar geometries and materials. The contact-impact behaviours of the pedestrian-vehicle interactions were determined from a series of impact tests with the vehicles and the bull bars being modelled. A generalised Hunt-Crossley damping model was fitted to the test data. The interaction models were implemented in MADYMO models of a vehicle pedestrian collision using the geometry of the vehicles and bull bars and a fiftieth percentile male human model. Head kinematics were extracted and the head impact severity estimated. The speed of the head impact with the bonnet was increased by between 7 and 55 percent in simulations where a bull bar was fitted to the vehicle. The increase in head impact velocity was not related to the bull bar material type. The 55 percent increase in head impact speed produced a 249 percent increase in HIC value, using a head-bonnet interaction model based on Australasian NCAP head impact test results. The location of the head impact was affected by the bull bar but the effect was not consistent. The simulation results show that the addition of a bull bar to the front of a vehicle increases the speed of the head impact with the bonnet. This speed increase appears to be less a product of the material the bull bar is made from, but more a product of the geometry of the bull bar. This suggests that bull bar geometries could be altered to improve pedestrian collision kinematics possibly even lessening the severity of the head impact with the bonnet. Combined with a soft material, such as polymer, this may lead to a safer bull bar designs for pedestrians.

KEYWORDS

Pedestrian crashes, Simulation, Bull bars, Injury risk

Summary

Vehicle frontal protection systems for motor vehicles (less prosaically referred to as bull bars or kangaroo bars) are a common addition to motor vehicles in Australia. A recent survey in Adelaide, South Australia, found that, at the sites typical of pedestrian crashes, bull bar equipped vehicles constitute around nine percent of the traffic; around half of all bull bars observed were fitted to high ground clearance SUV type vehicles (Anderson et al., 2008b). Hence, one might estimate that bull bars are involved in around 1 in 10 pedestrian crashes in South Australia.

The aim of this study was to assess the effect of bull bars on the kinematics of an adult pedestrian in a collision, to examine effects secondary to the impact between the pedestrian and the bull bar, particularly the effect on head impact kinematics. A further aim was to examine differential effects according to bull bar geometry and bull bar material (steel, alloy or plastic).

The contact-impact behaviour associated with the interaction between the a pedestrian and each bull bar and vehicle was identified from data collected for a separate study (Anderson et al., 2006) on the relative performance of bull bars and the fronts of vehicles in pedestrian subsystem tests. This contact-impact behaviour was then implemented into a MADYMO model of an adult pedestrian struck by a vehicle alone, and also with different types of bull bar.

The head impact velocity was consistently higher in simulations that included a bull bar, varying between 7 percent and 55 percent higher than the simulations with the vehicle alone. The average increase in the head impact velocity was 23 percent. There was no consistency in the increase in head impact velocity with regard to bull bar material.

The trajectory of the head was altered by the addition of a bull bar to the vehicle, but the effect on the trajectory varied from bull bar to bull bar. In some cases the head strike was closer to the leading edge but in others it was farther away.

A generic contact-impact model of the head-bonnet contact was used in all simulations. The addition of a bull bar to the front of the vehicles increased the HIC value produced by the head-bonnet contact in all simulations, in one case more than tripling the HIC value. It should be noted however, the generic stiffness definition means that the differences in the HIC values generated should be used to indicate trends in impact severity arising from the changes in head impact speed, rather than as applicable to the vehicles themselves.

Further work is needed to determine the specific geometric properties that contribute to an increase in head impact speed and their relative importance when compared to the bull bar's stiffness properties.

Contents

1 Introduction

Vehicle frontal protection systems for motor vehicles (less prosaically referred to as bull bars or kangaroo bars) are a common addition to motor vehicles in Australia. A recent survey in Adelaide, South Australia, found that, at the sites typical of pedestrian crashes, bull bar equipped vehicles constitute around nine percent of the traffic; around half of all bull bars observed were fitted to high ground clearance SUV type vehicles (Anderson et al., 2008b). Hence, one might estimate that bull bars are involved in around 1 in 10 pedestrian crashes in South Australia. Kloeden, White and McLean examined South Australian Coroner's records of pedestrian fatalities that occurred between 1991 and 1997, and found that bull bars were fitted to 8.8% of crash involved vehicles (Kloeden et al., 2000).

Impact tests have shown that the severity of the contact between the pedestrian and the bull bar is generally greater than it would be with the vehicle itself, but this is dependant on the material used to construct the bull bar: plastic bull bars are sometimes less aggressive than the vehicles to which they attach while steel bull bars can produce extremely high impact loads (Lawrence et al., 2000; Anderson et al. 2006). But bull bars might have other effects in pedestrian crashes too. They alter the front geometry of the vehicle and may therefore alter the kinematics of the struck pedestrian, either onto the upper surface of the vehicle, or onto the road.

The aim of this study was to assess the effect of bull bars on the kinematics of an adult pedestrian in a collision, to examine effects secondary to the impact between the pedestrian and the bull bar, particularly the effect on head impact kinematics. A further aim was to examine differential effects according to bull bar geometry and bull bar material (steel, alloy or plastic).

2 Methods

The methodology used in this study comprised two parts:

- The identification of the contact-impact behaviour associated with the interaction between the a pedestrian and each bull bar and vehicle, and
- The implementation of these into a MADYMO model of an adult pedestrian struck by a vehicle alone, and also with different types of bull bar.

The resulting models were analysed to examine variations in the kinematics of the pedestrian.

2.1 Contact-impact test data

The contact-impact models used in the models were generated from data collected for a separate study on the relative performance of bull bars and the fronts of vehicles in pedestrian subsystem tests. Details of that study are contained in a report by Anderson et al. (2006). The aim of that study was to report the performance of current bull bars and the vehicles to which they are fitted in tests designed to assess the risk that they pose to pedestrians. Tests were conducted at 30 km/h. They consisted of a child headform impact test on the top rail of the bull bar, and two upper legform impact tests: one on the top rail of the bull bar and one on the bumper of the bull bar. Equivalent tests were conducted on the vehicles themselves so that the relative performance of the bull bars could be assessed.

As the present study concerns the effect of the bull bar on the collision with an adult pedestrian, the results of the upper legform tests were used to estimate the contact-impact behaviour of each bull bar in an impact with a pedestrian. The data recorded in those tests were analysed to produce stiffness, damping and hysteretic characteristics that could be implemented in the multibody dynamics software code MADYMO (TASS, The Netherlands). The tests are shown schematically in Figure 2.1.

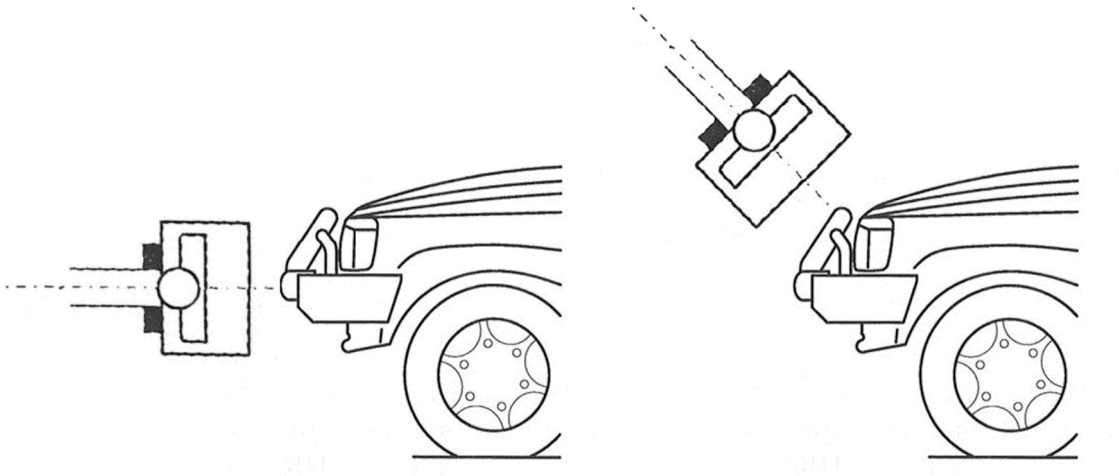

Figure 2.1
Upper legform test to the top rail (left) and bumper (right) used to determine the contact-impact behaviour of the bull bars and vehicles for the simulation

2.2 Vehicles and bull bars tested

Five types of high ground clearance vehicles were tested for this study. The bull bars tested were made from steel, alloy/aluminium or rotationally moulded polyethylene. The vehicles and bull bars tested are listed in Table 2.1. The aim was to test a range of bull bars that could be fitted to each of the five vehicles, so that some of the effects of bull bar material

and geometry on the impact behaviour could be measured. At the time of testing, polyethylene bull bars were unavailable for two of the five vehicles.

Table 2.1
Vehicles and bull bars tested

Vehicle	Steel bull bar	Aluminium / alloy bull bar	Polymer bull bar
Toyota Landcruiser	Aftermarket bumper replacement	OES bumper replacement	Not available at the time of testing
Nissan Patrol	OES bumper replacement	Aftermarket alloy nudge-bar	Aftermarket bumper replacement
Ford Courier	Aftermarket bumper replacement	OES bumper replacement	Aftermarket bumper replacement
Holden Rodeo	Aftermarket bumper replacement (note 1)	OES bumper replacement	Aftermarket bumper replacement
Toyota Hilux	OES bumper replacement	After market chassis mounted bar (note 2)	Not available at the time of testing

Notes:
1. The Holden Rodeo aftermarket steel bull bar was almost identical to the Toyota Landcruiser aftermarket steel bull bar. Tests were performed on the Landcruiser bull bar and the results were used for both bull bars.
2. The Toyota Hilux aftermarket alloy bull bar was almost identical to the Nissan Patrol aftermarket alloy bull bar, except for the addition of wing sections. Tests were performed on the Patrol bull bar and the results were used for both bull bars.

Impact locations varied from bull bar to bull bar, but in general, stiffer locations were selected, such as top rail locations adjacent to a bull bar stanchion, but with deference to the practicalities of testing: very stiff structures likely to saturate the instrumentation were avoided, as were parts of the bar liable to cause a glancing blow. A full description of impact locations can be found in the report on that study, Anderson et al. (2006).

Force data were acquired at 50 kHz per channel and conditioned according to CFC600 (SAE J211/1 - Instrumentation for Impact Test - Part 1 - Electronic Instrumentation). Legform velocity was measured just prior to contact with a dual-laser speed trap. All tests were recorded using high-speed digital video (1000 fps).

2.3 Contact-impact modelling (stiffness, damping and hysteretic characteristics)

The validity of the kinematics of the pedestrian model depends in part on the correct characterisation of interaction of the pedestrian and the vehicle in the simulation. This interaction is governed by the geometry of the vehicle/bull bar, and by the contact characteristics of the interaction. Of importance in the characterisation of the contact is the energy dissipated by each interaction, and the forces generated by each interaction.

In this study, contacts were modelled in a form consistent with Hunt-Crossley damping (Hunt and Crossley, 1975), as described in Anderson et al. (2008a). In this model of impact, damping is added in a more realistic way than is produced with a linear viscoelastic model of impact (Gilardi and Sharf, 2002; Muthukumar and DesRoches, 2006; Polukoshko, 2007). A characteristic of Hunt-Crossley damping is that the normal contact force is considered as a sum of elastic and damping forces, where the damping force is zero at the beginning and end of the impact and also at maximum penetration.

The Hunt-Crossley model of contact-impact is characterised by the following formulation:

$$F = K\delta^n + b\delta^p\dot{\delta}^q \quad (1)$$

where F is the normal contact force, δ is the contact penetration, K is the Hertzian elastic component of the contact force and b, p and q are constants. It is usual to set $p = n$ and

q = 1. Lankarani and Nikravesh (1990) showed that, in the case of Hertzian impact between two spheres, Equation 1 can be written:

$$F = K\delta^n \left[1 + c\dot{\delta}^q\right] \tag{2}$$

where c is a damping parameter.

Equations 1 and 2 make no allowance for energy dissipation due to plastic deformation. Lankarani and Nikravesh (1990) and others (as detailed by Goldsmith, 1960) proposed that the unloading behaviour of a Hertzian impact that includes permanent deformation could be described by

$$F = F_m \left[\frac{\delta - \delta_p}{\delta_m - \delta_p}\right]^n \tag{3}$$

where δ_p is the permanent deformation, δ_m is the maximum deformation, and F_m is the impact force at maximum deformation. As the impact velocity is zero at maximum penetration, an expression for the force at maximum penetration is $F_m = K\delta_m$. In this case, Equation 3 may be rewritten as

$$F = K\left[\frac{\delta_m}{\delta_m - \delta_p}\left(\delta - \delta_p\right)\right]^n$$

Which is a specific form of the Hertzian contact law. Damping can now be added in the unloading phase of such impacts in an analogous way as presented in Equation 3, i.e.:

$$F = K\left[\frac{\delta_m}{\delta_m - \delta_p}\left(\delta - \delta_p\right)\right]^n \left[1 + c\dot{\delta}^q\right] \tag{4}$$

A further generalisation of the damped loading and unloading phases of impact suggested by Equations 2 and 4 is given by

$$F = \begin{cases} F_{Elastic-load}\left[1 + c\dot{\delta}\right], & \dot{\delta} \geq 0 \\ F_{Elastic-unload}\left[1 + c\dot{\delta}\right], & \dot{\delta} \leq 0 \end{cases} \tag{5}$$

where $F_{Elastic-*}$ are numerically defined loading curves determined from an experimental test.

In the multibody simulation software package MADYMO, damping forces are calculated according to the following formula (adapted from TNO, 2007):

$$F_{Damping} = \left[c\dot{\delta} + f_{Damping}\left(\dot{\delta}\right)\right] f_{Amplification}\left(F_{Elastic}\right)$$

Where $f_{Damping}$ and $f_{Amplification}$ are functions of the penetration velocity and the elastic force, respectively.

The total normal force is:

$$F_{Normal} = F_{Elastic} + \left[c\dot{\delta} + f_{Damping}\left(\dot{\delta}\right)\right] f_{Amplification}\left(F_{Elastic}\right) \quad (6)$$

By defining $f_{Amplification}\left(F_{Elastic}\right) = F_{Elastic}$ and $f_{Damping}\left(\dot{\delta}\right) = 0$ the total force can be written as

$$F_{Normal} = F_{Elastic}\left[1 + c\dot{\delta}\right] \quad (7)$$

where $F_{Elastic}$ is numerical force-deformation characteristic defined separately in the loading and unloading phases of the contact. Equation 7 is consistent with Equation 5, allowing the implementation of a contact-impact model based on Hunt-Crossly damping with permanent indentation.

Such a modelling approach was validated by Anderson et al. (2008a), and subsequently has been successfully used to characterise test data describing the contact between impactors and vehicles structures (unpublished results).

In this study, impact test data with bull bars and the vehicles were modelled according to Equation 5. After obtaining an estimate of the normal force-deformation loop from the experiment, values of the damping parameter were trialled (c^*). The corresponding trial elastic loading and unloading functions ($F^*_{Elastic}$) were determined by plotting $F^*_{Elastic} = F_{Normal} / \left[1 + c^*\dot{\delta}\right]$, adjusting the trial value of until all apparent damping was accounted for; this was apparent when the characteristic of $F^*_{Elastic}$ was such that the peak elastic force occurred at maximum penetration. (For more detail, see Anderson et al., 2008a). The resulting elastic unloading force was used in conjunction with Hysteresis Model 3A.

An advantage of modelling the contact-impact behaviour in this way is that rate effects are properly accounted for, which is important when the simulated contact conditions (effective mass and speed) vary from that in the test used to determine the contact behaviour.

2.4 Multibody modelling

All vehicles tested had been obtained for testing by the Australasian New Car Assessment Program. Vehicle dimensions were obtained for the purposes of the ANCAP tests using a prism-less digital theodolite. For the present purpose, scaled photographs of the vehicles were also used to provide further data on the bumper geometry. Bull bar geometry was measured directly from exemplar bull bars. The position of each bull bar relative to the vehicle to which it attached was scaled from photos taken at the time of testing. Consistently, the centre of the bull bar top rail was around 100 mm in front of the front-most point of the leading edge of the vehicle, and this position was used in all MADYMO models (Figure 2.2). The geometry of each bull bar was defined in MADYMO using a combination of cylinders and planes. For the round bar sections cylinders of the 2nd degree were used and for the plate sections either a cylinder of degree 10 or a plane were used, depending on the orientation, and the nature of the modelled interaction between the pedestrian and the bull bar.

2.5 MADYMO human body modelling

The model that was used for the simulation part of this study was developed specifically to simulate pedestrians in car-pedestrian collisions. The model has been presented previously (Garrett, 1996; Garrett, 1998), and used for accident simulation purposes (Anderson et al., 2002; Anderson et al., 2005; Anderson et al., 2007). The model consists of 17 rigid

segments linked by kinematic joints that are largely based on the model proposed by Ishikawa et al. (1993) although some joints have been added while others have been modified.

The model represented a 50th percentile male (for weight and weight) with segment lengths, masses and moments of inertia generated from the GEBOD anthropometric database (Baughman, 1983).

The model was positioned laterally to the vehicle as illustrated in Figure 2.2.

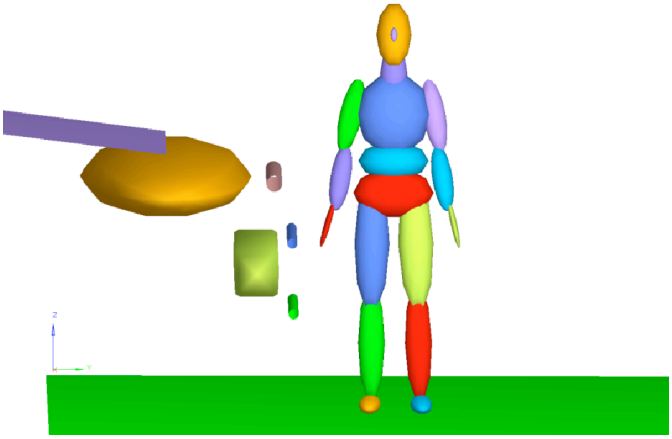

Figure 2.2
Pedestrian orientation in the simulations

2.6 MADYMO model runs and outputs

The speed of the vehicle in the simulation was modelled as that of a typical SUV type vehicle performing an emergency 'brake to stop' manoeuvre (0.7 g deceleration). The initial velocity was set to 30 km/h in all simulations. The difference in impact velocity (at first contact) attributable to the difference in geometry introduced by the bull bars was about 0.17 m/s.

To an enable an estimate of head impact severity, a contact-impact model derived from an Australian New Car Assessment Program headform impact test was used. The test chosen was a child headform test that produced a HIC value of 1991 (mass = 2.5 kg, speed 11.1 m/s). The test was analysed using the procedure, described earlier, for characterising the bull bar tests. A numerical elastic loading and unloading function was defined according to Equ. 5 after a suitable damping parameter had been identified. The resulting contact-impact model was:

$$F = \begin{cases} K\delta^{1.5}\left[1 + c\dot{\delta}\right], & \dot{\delta} \geq 0 \\ K\left[\dfrac{\delta_m}{\delta_m - \delta_p}\left(\delta - \delta_p\right)\right]^{1.5}\left[1 + c\dot{\delta}\right], & \dot{\delta} \leq 0 \end{cases}$$

where K = 2.84e5, n = 1.5, c = 0.33, δ_m = 0.0389, δ_p = 0.033.

3 Results

3.1 Stiffness, damping and hysteretic characteristics of bull bars and vehicle leading edges

The force-deflection traces from all impact tests with the leading edges of the vehicles and the top bars of all bull bars are shown in Figure 3.1, and the force-deflection traces from the test with the bumpers are shown in Figure 3.2. (Note that the vertical scales in these Figures vary.)

In fitting the damped model of contact impact to the data, a Hertzian elastic stiffness could be defined in the loading and unloading phase in for most characteristics. For other impacts where a Hertzian stiffness was a poor fit, numerical definitions of the elastic loading and unloading characteristics were defined. In some cases where there was significant resonance in the contact, a Hertzian stiffness was defined such that the model produced a correct peak load and energy dissipation — mostly these type of contacts occurred in top-rail impacts with alloy bull bars. In all cases, care was taken to ensure that the coefficient of restitution and the time history of the work done in the contact was a close match to that which was measured in the impact test.

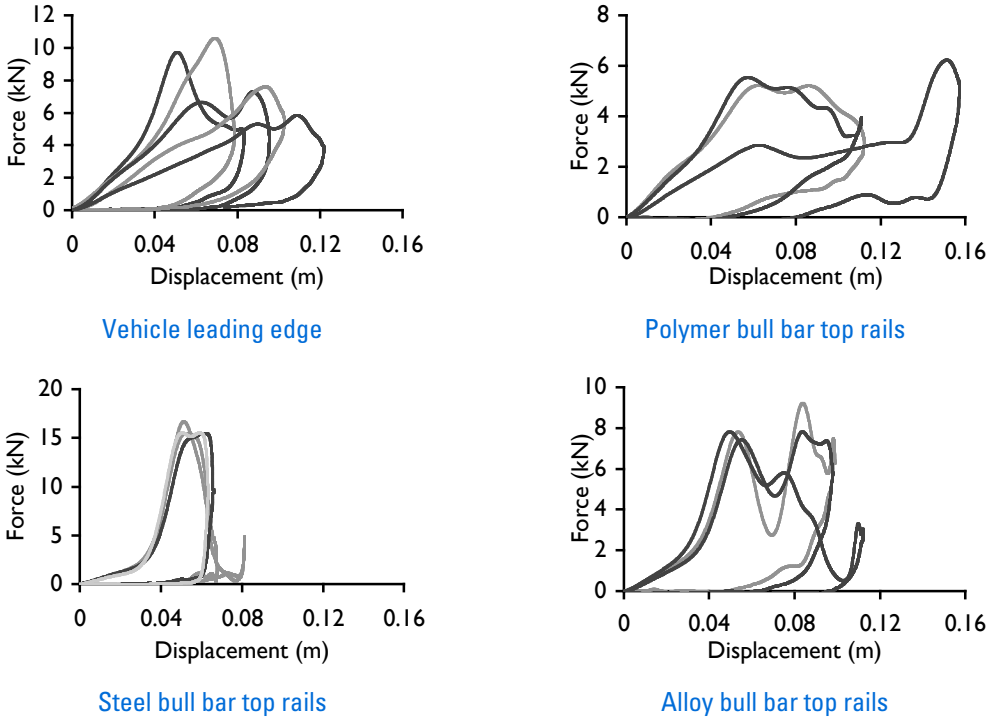

Figure 3.1
Force-deflection of the leading edge of vehicles and top bars of bull bars.

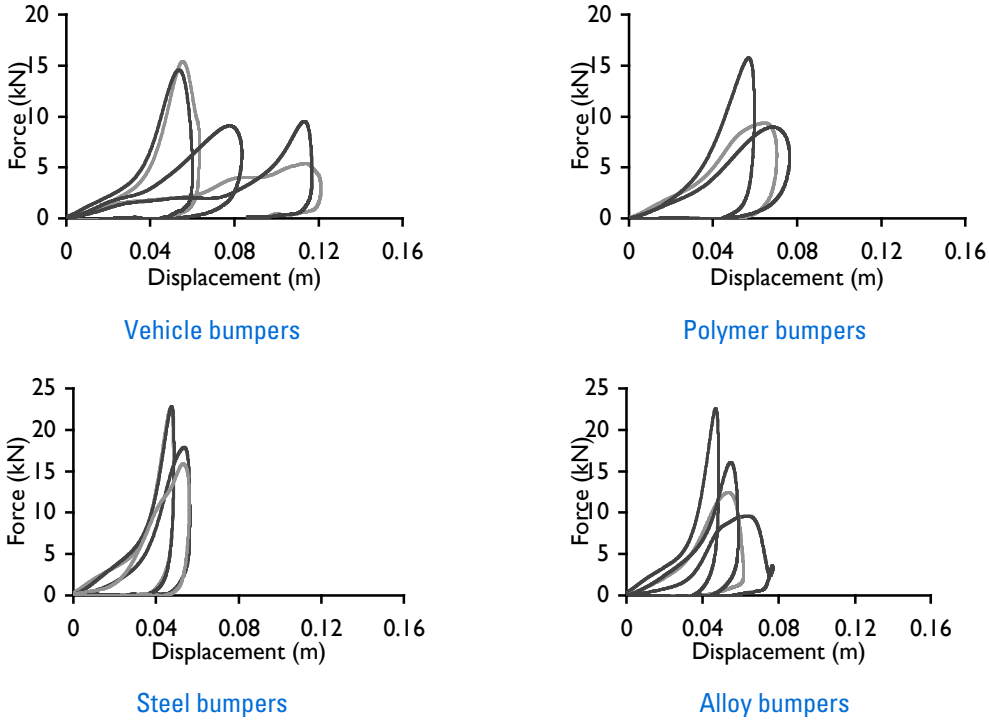

Figure 3.2
Force-deflection of the bumpers.

3.2 Effect on head impact velocity

The results for the head impact velocity relative to the vehicle are shown in Table 3.1. The head impact velocity was consistently higher in simulations that included a bull bar, varying between 7 percent and 55 percent higher than the simulations with the vehicle alone. The average increase in the head impact velocity was 23 percent. There was no consistency in the increase in head impact velocity with regard to bulbar material.

Table 3.1
Head CoG velocity at Impact with Bonnet (m/s) and the head impact speed as a percentage of the no bull bar simulation head impact speed

Vehicle	No bull bar		Polymer bull bar		Alloy bull bar		Steel bull bar	
Ford Courier	6.08	(100%)	6.57	(108%)	7.31	(120%)	6.51	(107%)
Toyota Hilux	5.35	(100%)	-	-	7.81	(146%)	8.30	(155%)
Toyota Landcruiser	6.34	(100%)	-	-	6.93	(109%)	7.47	(118%)
Nissan Patrol	5.38	(100%)	8.01	(149%)	6.91	(128%)	6.36	(118%)
Holden Rodeo	7.21	(100%)	8.29	(115%)	8.10	(112%)	8.20	(114%)

Figure 3.3 shows the horizontal component of the relative head velocity plotted against the vertical component of the relative velocity of the head centre-of-gravity for all simulations involving the Ford Courier. The head impact velocity is indicated with an "o". In this plot, the radial lines display values of the resultant speed. The polar velocity plots for the other vehicles can be found in Appendix A.

The higher velocity trajectories of the simulations that involved a bull bar can be clearly seen: the velocity is higher throughout the simulation and upon head impact.

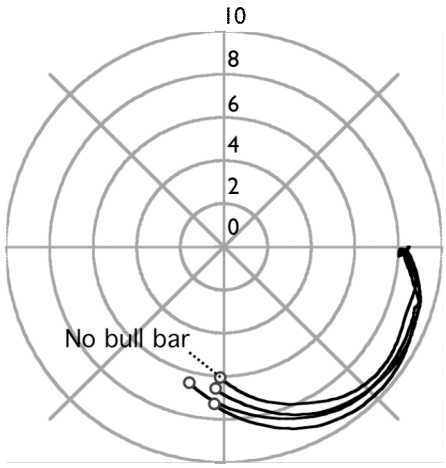

Figure 3.3
Polar plot showing the speed and angle of the head CoG until the point of impact in simulations involving the Ford Courier

Figure 3.4 shows the same velocity data as Figure 3.3, but plotted against time. (The plots of head speed over time for the simulation of the other vehicles can be found in Appendix B.) As one would expect, the speed of head in the non-bull bar simulation rises and peaks later than the simulations without bull bars. The head also strikes the bonnet later than when a bull bar is not present. This appears to be one reason for the lower head impact velocity.

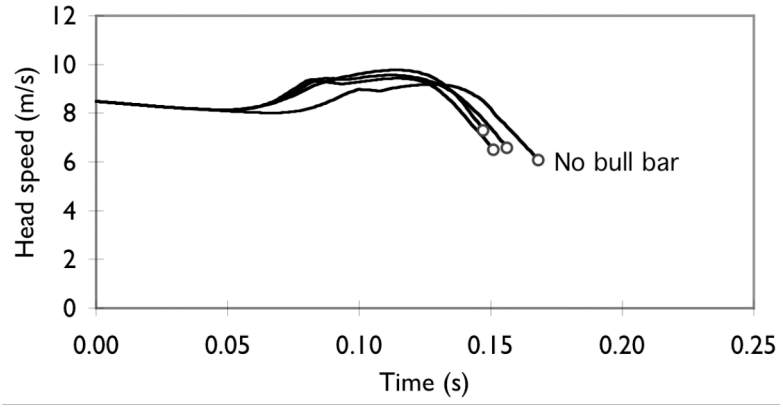

Figure 3.4
Velocity-time plot of the head CoG for simulations involving the Ford Courier

3.3 Effect on head impact location

Figure 3.4 shows the trajectory of the head centre-of-gravity relative to the vehicle up until impact with the bonnet for all simulations involving the Ford Courier. (The head trajectory plots for the other vehicles can be found in Appendix C.) The trajectory transformation was calculated such that the origin of the vehicle frame was at ground level directly under the front-most point on the bumper. Here the effect of the presence of a bull bar was less than the variation between bull bar types.

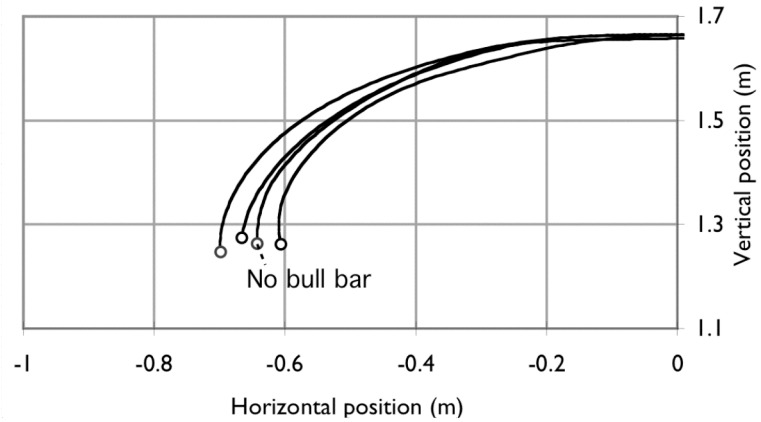

Figure 3.5
Trajectory of the Head CoG relative to the vehicle in simulations involving the Ford Courier

3.4 Effect on head impact severity

Table 3.1 showed that the head's velocity at impact is greater when a bull bar is fitted. The differences in the head impact speed do not in themselves indicate the differences in head injury risk. To estimate these differences the Head Injury Criterion (HIC) was calculated for each simulation. The stiffness definition was based on an Australasian NCAP child headform test that produced a HIC of 1991 with a head mass of 2.5 kg, and speed of 11.1 m/s. In these simulations, the effective head mass was higher and head speed was lower, producing smaller HIC values. The force-displacement loop produced in the simulation is illustrated in Figure 3.6. This characteristic was from the simulation with the highest impact speed.

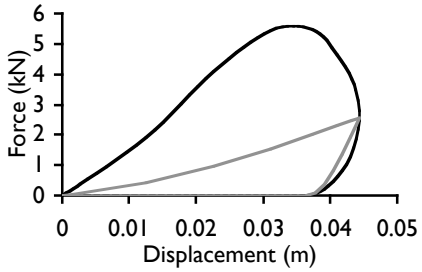

Figure 3.6
Force displacement curve produced by the head impact with the bonnet in the simulation of the Toyota Hilux with a steel bull bar. The elastic component of the contact force is shown in grey and the total force including damping in shown in black.

The resulting estimates for HIC are given in Table 3.2. The HIC values increased for all simulations where the bull bar was fitted The increases were as large as 219 per cent, corresponding to a 55 per cent increase in head strike velocity. The average increase in the HIC value was 59%.

Table 3.2
HIC results for head-bonnet impact

Vehicle	No Bull Bar	Polymer bull bar	Alloy bull bar	Steel bull bar
Ford Courier	360	400	420	440
Toyota Hilux	250	-	573	798
Toyota Landcruiser	385	-	484	575
Nissan Patrol	307	628	556	446
Holden Rodeo	471	543	593	596

4 Discussion

The kinematics of the pedestrian model were altered by the addition of a bull bar to the front of the vehicle. The presence of the bull bars in the simulations increased the head speed of the pedestrian model at impact when compared to the vehicle with no bull bar fitted. The magnitude of this increase varied from bull bar to bull bar and does not appear to be solely related to the material the bull bar is manufactured from. This suggests that it is also related to the individual combinations of vehicle and bull bar geometry rather than the material used in the bull bar's construction.

The trajectory of the head was altered by the addition of a bull bar to the vehicle, but the effect on the trajectory varied from bull bar to bull bar. In some cases the head strike was closer to the leading edge but in others it was farther away.

A generic contact-impact model of the head-bonnet contact was used in all simulations. This contact-impact model was defined using Hunt-Crossly damping applied to a Hertzian contact stiffness that had been fitted to head impact data recorded in a test with one of the vehicles. The addition of a bull bar to the front of the vehicles increased the HIC value produced by the head-bonnet contact in all simulations, in one case more than tripling the HIC value. It should be noted however, the generic stiffness definition means that the differences in the HIC values generated should be used to indicate trends in impact severity arising from the changes in head impact speed, rather than as being applicable to the vehicles themselves.

The limitations of the methodology used to produce the results reported here lie both in the testing and modelling. The EEVC WG17 upper legform was used for the testing. It was assumed that this legform represents the stiffness and damping properties of the lower extremities in an impact with a vehicle. This is only an assumption and may be a source of error. An improvement in the contact-impact modelling may be to subtract the contact properties of the upper legform and too incorporate the contact properties of the human lower extremity into the characteristic instead.

The high speed video of the top bar impact showed that, in some tests, the bull bar pivots about the lower stanchion support during the loading phase. This behaviour has been modelled in MADYMO within the contact definition – therefore, in the simulations, the geometry may be more fixed than is realistic. The effects of potential errors in the effective geometry of the bull bar were checked in several simulations by moving the location of the top bar by 50 mm vertically, up and down. These trials had negligible effect on the results, and so it appears that the approximation inherent in our modelling approach has little effect.

5 Conclusion

The results of this study show that the addition of a bull bar to the front of a vehicle increases the speed of the head impact with the bonnet. This speed increase appears to be less a product of the material the bull bar is made from but a product of the geometry of the bull bar. The result is that, in an impact with a bonnet of typical properties, the impact severity can be markedly increased. Further work is needed to determine the specific geometric properties that contribute to an increase in head impact speed and their relative importance when compared to the bull bar's stiffness properties.

Acknowledgements

This study was funded by the South Australian Motor Accident Commission through a Project Grant to the Centre for Automotive Safety Research.

The Centre for Automotive Safety Research receives core funding from both the South Australian Department for Transport, Energy and Infrastructure and the South Australian Motor Accident Commission.

References

Anderson R, McLean AJ, Streeter L, Ponte G, Sommariva M, Lindsay T, Wundersitz L (2002) Severity and type of pedestrian injuries related to vehicle impact locations and results of sub-system impact reconstruction, Proc. 2002 International IRCOBI Conference on the Biomechanics of Impact, pp 289-299.

Anderson, R.W.G., Long, A.D., Serre, T. (2008) Continuous contact-impact modelling for multi-body simulations of pedestrian-vehicle contact interactions based on experimental data. J. of Nonlinear Dynamics (under review).

Anderson, R. W. G., McLean, A. J. and Dokko, Y. (2005) Determining accurate contact definitions in multi-body simulations for DOE-type reconstruction of head impacts in pedestrian accidents, Proc. 19th International Conference on the Enhanced Safety of Vehicles, Paper 05-0175.

Anderson, R.W.G., Ponte, G., Doecke, S. (2008) A survey of bull bar prevalence at pedestrian crash sites in Adelaide, South Australia. Centre for Automotive Safety Research, Adelaide, South Australia.

Anderson RWG, McLean AJ, Ponte G, Streeter L (2007) Pedestrian reconstruction using multibody MADYMO simulation and the Polar-II dummy: a comparison of head kinematics, Proc. 20th International Technical Conference on the Enhanced Safety of Vehicles, Paper 07-0273-0

Anderson R. W. G., van den Berg A. L., Ponte G., Streeter L. D., McLean A. J. (2006) Performance of bull bars in pedestrian impact tests. Centre for Automotive Safety Research, Adelaide, South Australia.

Baughman, L. (1983) Development of an Interactive Program to Produce Body Description Data, Report no. AFAMRL-TR-83-058, US Air Force Aerospace Medical Research Laboratory. Biomechanics of Impact, pp. 159-174.

Garrett, M. (1996) Head impact modelling using computer accident simulation based on cadaver records. Proc. 24th International workshop on human subjects for biomechanical research, pp. 81-92.

Garrett, M. (1998) Head impact modelling using MADYMO simulations of documented pedestrian accidents. Proc. Conference on Pedestrian Safety, pp. 158-168.

Gilardi G., Sharf, I. (2002) Literature survey of contact dynamics modelling. Mechanism and Machine Theory, Vol. 37(10), pp. 1213—1239.

Goldsmith, W.: Impact: The Theory and Physical Behaviour of Colliding Solids. Edward Arnold, London (1960).

Hunt, K.H., Crossley, F.R. (1975) Coefficient of restitution interpreted as damping in vibroimpact. J. Appl. Mech, Vol 42(E), pp. 440—445,.

Ishikawa H., Kajzer J., Schroeder G. (1993), Computer simulation of impact response of the human body in car-pedestrian accidents, Proc. 37th Stapp Car Crash Conference, pp 235 - 248

Kloeden, C. K., White K., and McLean, A. J. (2000) Characteristics of Fatal and Severe Pedestrian Accidents in South Australia, for Transport SA, Adelaide, South Australia.

Lankarani, H.M., Nikravesh, P.E. (1990) A contact force model with hysteresis damping for impact analysis of multi-body systems. J. Mech. Des., Vol. 112: pp. 369—376.

Lawrence G., Rodmell C., Osborne A. (2000) Assessment and test procedures for bull bars, TRL report 460, Transport Research Laboratories, Crowthorne, Berkshire, United Kingdom.

Muthukumar, S. and DesRoches, R. (2006) A Hertz contact model with non-linear damping for pounding simulation, Earthquake Engng Struct. Dyn., Vol. 35, pp. 81 – 828.

Polukoshko, S., Viba, J., Kononova, O., and Sokolova S. (2007) Rigid body impact models partially considering deformation, Proc. Estonian Academy of Science and Engineering, Vol. 13, 2, pp. 140-155.

Appendix A - Polar plots of speed and angle of the head CoG

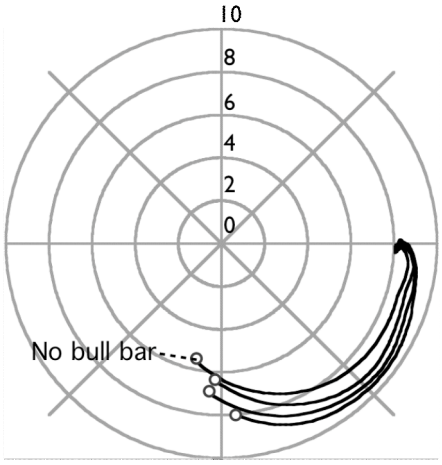

Patrol

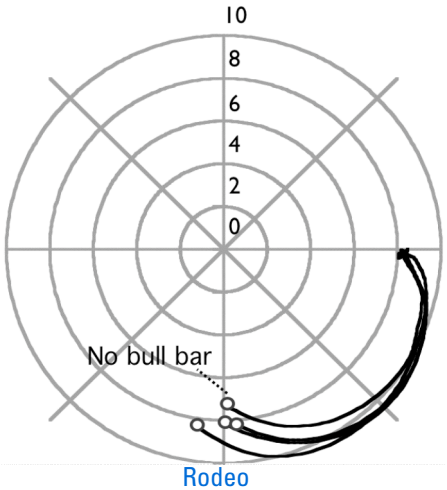

Rodeo

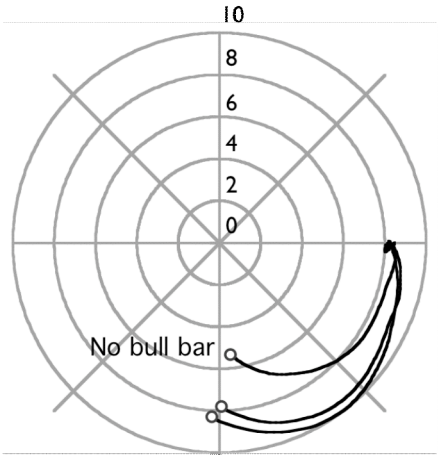

Hilux

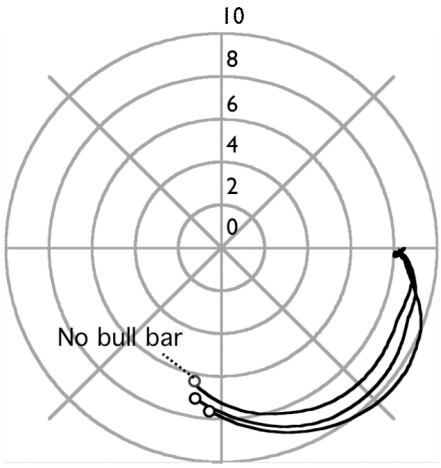

Landcruiser

Figure A1: Polar plots showing the speed and angle of the head CoG until the point of impact

Appendix B - Velocity-time plots of the head CoG

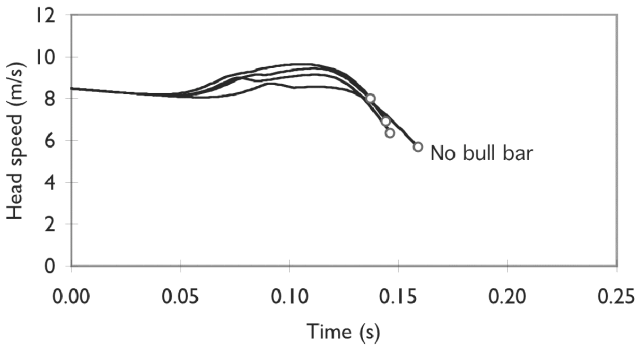

Patrol

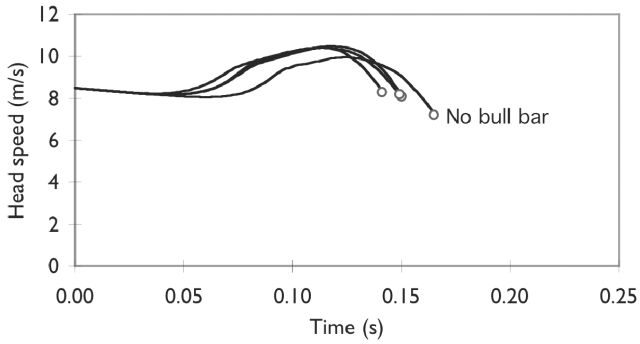

Rodeo

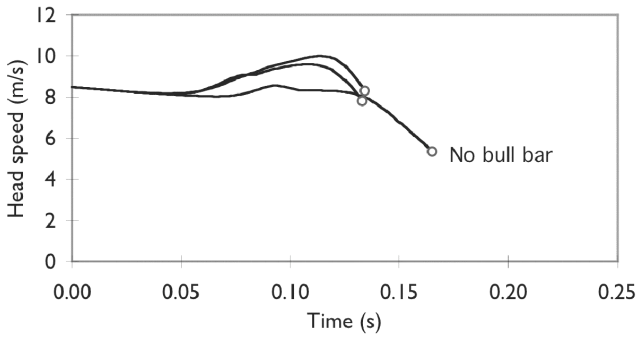

Hilux

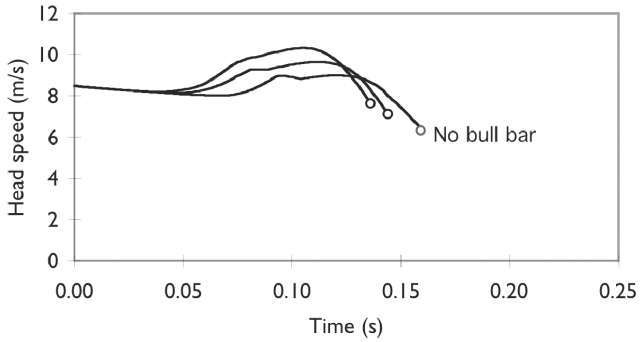

Landcruiser

Figure B1: Velocity-time plots of the head CoG

Appendix C - Trajectories of the head CoG relative to vehicle

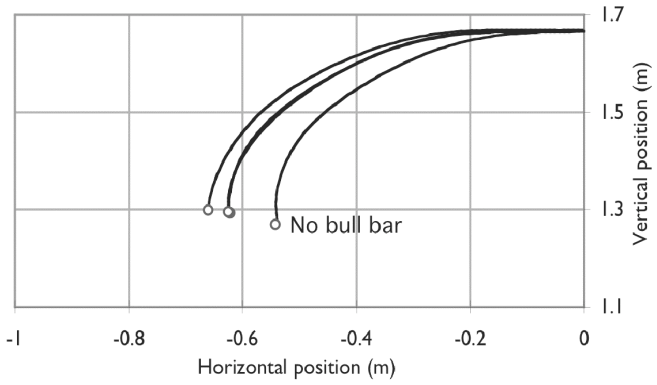

Patrol

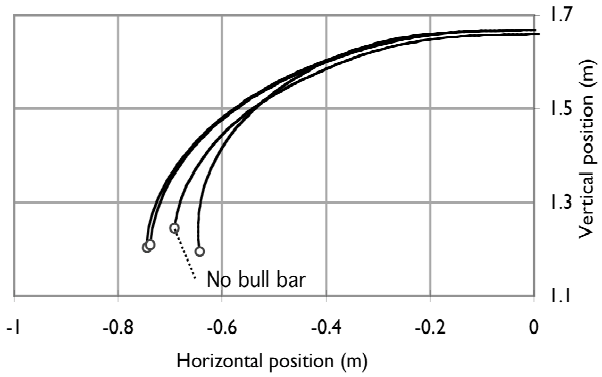

Rodeo

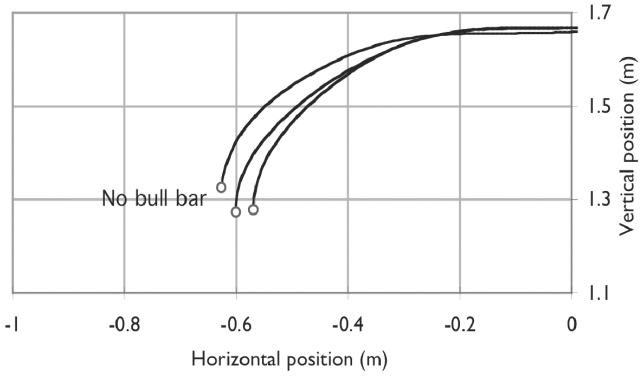

Hilux

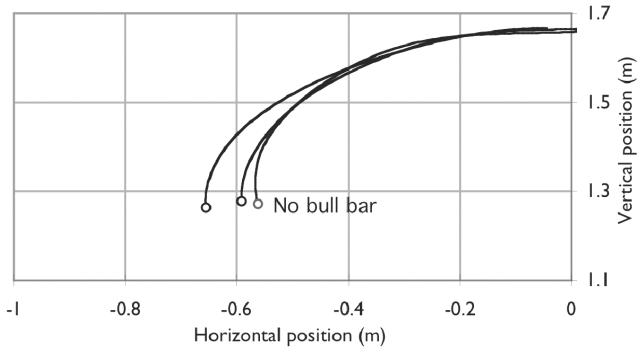

Landcruiser

Figure C1: Trajectories of the Head CoG relative to the vehicle